Materials and Design 88 (2015) 1326–1333

Contents lists available at ScienceDirect

Materials and Design

journal homepage: www.elsevier.com/locate/jmad

Effect of alloy design on improving toughness for X70 steel during welding

Zhixiong Zhu *, Jian Han *, Huijun Li

School of Mechanical, Materials & Mechatronic Engineering, University of Wollongong, Wollongong, NSW 2522, Australia

ARTICLE INFO

Article history:
Received 25 June 2015
Received in revised form 11 September 2015
Accepted 14 September 2015
Available online 16 September 2015

Keywords:
Electron microscopy
Mechanical characterisation
Ferrous alloy
Precipitation
Fracture
Welding

ABSTRACT

To identify and determine the optimal alloy design of Ti, the toughness in simulated coarse-grained heat affected zone (CGHAZ) of API 5L grade X70 steels with Ti/N ratios ranged from 1.9 to 4.9 was evaluated using Charpy V-notch (CVN) testing and crack tip opening displacement (CTOD) testing. A Gleeble 3500 thermo-mechanical simulator was utilised to produce the simulated CGHAZ with equivalent heat input of 2.5 kJ/mm. The CGHAZ microstructures including prior austenite grain size and precipitation were examined using optical microscope (OM), scanning electron microscope (SEM) and transmission electron microscope (TEM). The results show that the microstructural constituents in the simulated CGHAZ for different Ti/N ratios consisted of bainitic ferrite and a small amount of martensitic-austenitic (M-A) constituents. In the studied range of Ti/N ratios, the statistical analysis of precipitates revealed that Ti/N ratio has little influence on the average precipitation size, which was controlled in a tight range (52–57 nm). However, at near-stoichiometric Ti/N ratio, higher number density of precipitates in the simulated CGHAZ certainly contributed to the finer austenite grain size and hence improved CGHAZ toughness performance.

1. Introduction

As the increase of energy consumption year by year, pipeline steels are developed towards high strength, superior toughness and excellent weldability for the efficient use of materials [1–5]. Among of all, the toughness is a key factor that restricts the extensive applications of high strength pipeline steels in the energy industry [6]. It is known that utilisation of thermo-mechanical controlled processing (TMCP) can significantly refine the grains. Thus, a combination of high strength and excellent toughness can be achieved in the base metal (BM). However, during the welding process, the desirable microstructure obtained in the BM can be modified by the severe welding thermal cycles. The weld heat affected zone (HAZ), especially the coarse-grained HAZ (CGHAZ), exhibits much lower toughness compared with the BM, due to the loss of the grain boundary pinning effect from microalloying precipitates and hence the occurrence of grain coarsening in this region.

The CGHAZ is considered to be the most critical region within the weld HAZ for single pass welds and largely determines the toughness, especially for high heat input welds. Considerable efforts have been made to evaluate the fracture toughness in the HAZ of pipeline steels using numerous testing methodologies [7–12]. The values from Charpy V-notch (CVN) testing and crack tip opening displacement (CTOD) testing have been regarded as important indexes to assess the toughness of steel materials. CVN testing was extensively used as a pre-qualification method for the evaluation of HAZ toughness due to the advantages of simple sample preparation, inexpensive testing procedures and easy data analysis [12–14]. On contrast, CTOD testing, as a fracture mechanics based method, is complicated but better for the understanding of fracture mechanics [15,16]. The CTOD testing, which is sensitive to the fracture initiation and propagation, can reveal the local brittle zone as evidenced by the presence of "pop-in" in the displacement-time curve [17–19].

There have been numerous factors in controlling the CGHAZ toughness, including welding parameters, phase transformation, etc. However, the grain growth in the CGHAZ is the main concern. Small addition of Ti is beneficial to grain size control in the CGHAZ, as TiN precipitates with high thermal stability, can form and pin the grain boundaries at high temperature, thereby restricting austenite grain growth in the CGHAZ. The variations in Ti, N concentrations and Ti/N ratios are essential for the control of mechanical properties in the CGHAZ. However, the optimal levels of Ti, N and Ti/N ratio are controversial in the open literatures [20–23]. Different published research work carried out previously in an attempt to identify the optimal Ti, N levels and Ti/N ratios were very different and sometimes even contradict, due to the various discrepancies (for example, the alloy design, thermal history, experimental conditions, etc.) [24]. Moreover, this topic is still not in good agreement in international standards and during the procurement of line pipes. US pipeline specifications API 2W and API 2H set a limit of Ti level to below 0.02 wt.% and the recommended

* Corresponding authors at: Faculty of Engineering & Information Sciences, University of Wollongong, Northfields Avenue, Wollongong, NSW 2522, Australia.
E-mail addresses: zz056@uowmail.edu.au (Z. Zhu), jh595@uowmail.edu.au (J. Han).

http://dx.doi.org/10.1016/j.matdes.2015.09.073
0264-1275/

Ti/N ratio is 2; API 5L allows maximum 0.06 wt.% of Ti additions with no particular control of Ti/N ratio. Furthermore, Australian Standard AS2885 does not address this issue at all.

In this context, for better understanding the significance of Ti/N ratio on the precipitation behaviour and fracture toughness in the HAZ, a series of API 5L grade X70 steels with different Ti/N ratios were investigated. The steels were subjected to a welding thermal cycle experienced in the CGHAZ with equivalent heat input of 2.5 kJ/mm. The microstructure and precipitates in the simulated CGHAZ were also observed. Meanwhile, the toughness of simulated CGAHZ was assessed using CVN and CTOD testing. The influence of precipitate distribution on the microstructural evolution and toughness of the CGHAZ will be discussed in the present paper.

2. Experiments

A series of API 5L grade X70 steels containing different Ti, N concentrations and various Ti/N ratios but otherwise almost identical were investigated. The chemical compositions of the studied steels are shown in Table 1. The Ti/N ratio ranges from 1.9 to 4.9. These steels display good strength properties (yield strength: 520–605 MPa; tensile strength: 595–675 MPa) and excellent low temperature toughness (CVN impact energy >200 J at −40 °C), which satisfies the requirements of pipeline specifications. The superior balanced mechanical properties are due to the formation of fine ferritic microstructure during TMCP. The BM microstructure of different Ti/N ratios was very similar, and the typical microstructure for these steels is shown in Fig. 1, which consists of fine polygonal ferrite with a small amount of pearlite islands discontinuously distributed along the ferrite grain boundaries. The average ferrite grain size was approximately 5 μm, and the Vickers hardness (load: 1 kg) was approximately 195 HV_1.

To evaluate the microstructure and mechanical properties in the CGHAZ, the samples with dimensions of 10 × 10 × 75 mm^3 (for CVN testing) and 10 × 20 × 92 mm^3 (for CTOD testing) for weld HAZ thermo-mechanical simulations were machined from the studied steels with thickness of 14.1 mm. The weld HAZ simulations were carried out using a Gleeble 3500 thermo-mechanical simulator. After several trials of different free spans, a 15 mm free span was chosen for thermal cycles to provide a relatively wide thermally cycled zone with homogeneous microstructure and properties of CGHAZ. The simulation sample configuration and simulation schedule are illustrated in Fig. 2. The simulation was performed in a vacuum chamber to minimise the oxidation on the sample surface. The processing involved heating the samples to 1350 °C, holding for 0.5 s and controlled cooling to 200 °C with cooling time from 800 °C to 500 °C to be 38.5 s (equivalent heat input of 2.5 kJ/mm). For accurate control of temperature, K-type thermocouples were spot welded in the middle of the sample surface. In addition, before performing microstructural analysis and mechanical testing, microstructural observations of the samples for CGHAZ simulation trials suggested that the regions subjected to the desirable CGHAZ thermal treatment at the sample mid length were approximately 7 mm and 3.5 mm for both CVN and CTOD specimens respectively.

One sample of each studied steel experienced CGHAZ simulation was selected for microstructural analysis. The samples were cut from the middle where the thermocouples were located. Then the middle cross-section was mounted with resin, grinded and polished to 1 μm. Afterwards, the samples were etched in 2 vol.% HNO_3 in ethanol solution

Table 1
The chemical compositions of the studied API 5L grade X70 steels (in ppm for Ti and N contents; in wt.% for others).

Steel	C	Si	Mn	Mo	V	Nb	Ti	N	Ti/N	Ni + Cr + Cu
1	0.045	0.22	1.60	0.146	0.023	0.052	60	32	1.9	0.38
2	0.047	0.23	1.62	0.144	0.023	0.055	87	27	3.2	0.37
3	0.051	0.22	1.57	0.150	0.024	0.055	83	17	4.9	0.38

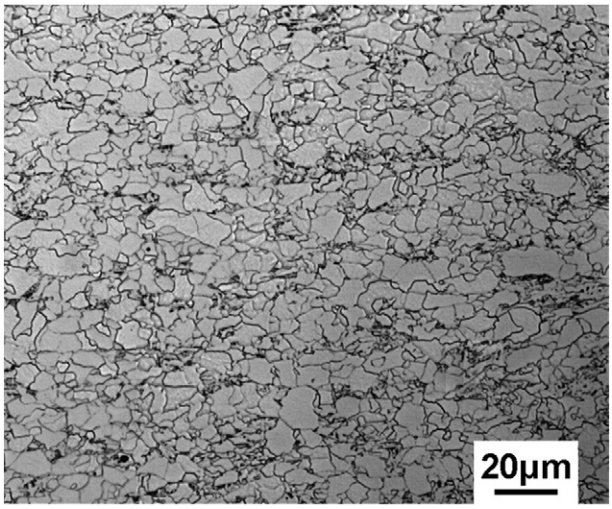

Fig. 1. The typical microstructure of the BM for the studied X70 grade steels.

to reveal the microstructure and then observed using JEOL 6490 scanning electron microscope (SEM) and 7001F field emission gun SEM for high magnification observation of precipitates. After the SEM microstructural examination, the samples were re-polished and etched in picric acid at 68 °C to reveal the prior austenite grain boundaries. Then

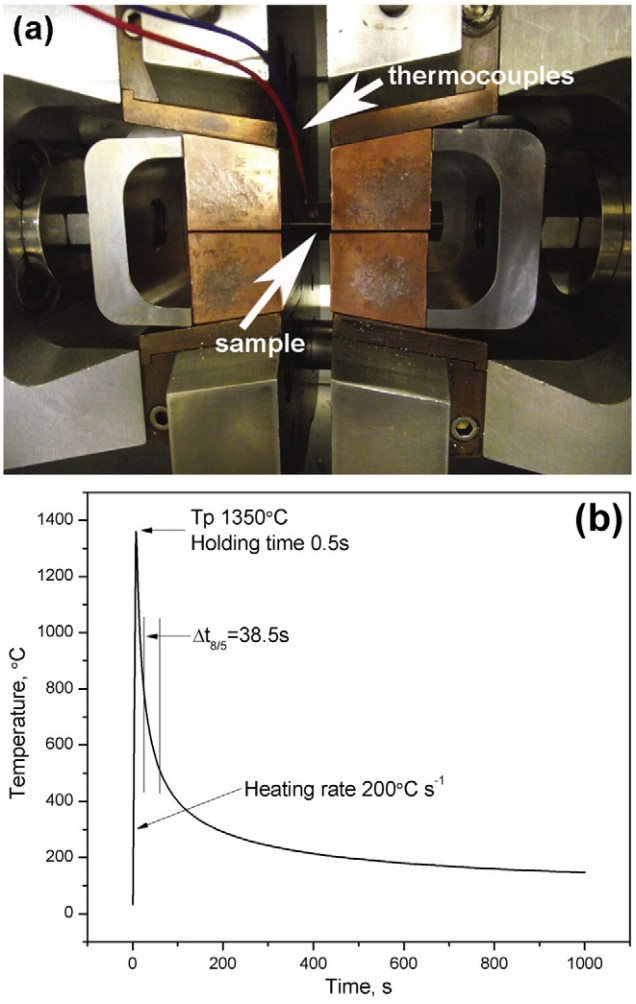

Fig. 2. CGHAZ simulation using a Gleeble 3500 simulator: (a) sample chamber showing the simulation configuration; (b) the welding thermal cycle employed for the simulation of CGHAZ.

the samples were observed using a Leica DMR optical microscope (OM). The prior austenite gran size was measured using planimetric method and thus statistically analysed.

To further characterise the precipitates, the fresh etched surfaces (etched with 2 vol.% nital) were coated with carbon in a vacuum chamber for the preparation of carbon replicas. The extraction of the precipitates embedded in the carbon film was performed in 8 vol.% HNO_3 in ethanol solution. After the extraction process, Cu-grids with a diameter of approximately 3 mm were used to support the carbon films. Finally, the replicas were analysed using a JEOL 2011 transmission electron microscope (TEM). The precipitate size was measured using an image analyser.

The Vickers hardness for the simulated samples was measured on a DuraScan 70 hardness tester with a load of 1 kg. Five measurements were recorded for each sample and the average values were regarded as the hardness values. The simulated samples with size of $10 \times 10 \times 75$ mm^3 were shortened to 55 mm in length and V-notched with T-L orientation according to ASTM E23. The CVN testing was conducted on an Instron Charpy impact tester. For CTOD testing, the samples with size of $10 \times 20 \times 92$ mm^3 were precisely notched and precracked with T-L orientation based on ISO 12135. Both the CVN and CTOD testing was conducted at temperature of −20 °C. For each sample, three valid tests were used for both CVN and CTOD testing to calculate the average values and standard deviations. The impact energies and CTOD values of the simulated CGHAZ were recorded during the testing. The fracture locations of all tested samples did not beyond the CGHAZ treated region at the sample mid length, which ensures the reliable and accurate tests. Finally, the fracture surfaces were analysed by using a JEOL 6490 SEM.

3. Results

3.1. OM & SEM study of microstructure

The SEM micrographs with low and high magnifications of simulated CGHAZ for the studied X70 steels are shown in Fig. 3. From the low magnification micrographs (Fig. 3a, c & e), the steel microstructure mainly consisted of bainitic ferrite with morphology of parallel laths aligned within the prior austenite grains and a small amount of M-A islands discontinuously distributed between the ferrite laths. Also, precipitates of microalloying elements were observed in the high magnification SEM micrographs (indicated by white arrows in Fig. 3b, d & f). The influence of Ti/N ratio on the microstructure constituents was not apparent in the studied range of Ti and N levels. To further investigate the influence of Ti/N ratios, the prior austenite grain size in the simulated CGHAZ was statistically analysed. As shown in Table 2, the simulated CGHAZ of Steel 2 with near-stoichiometric Ti/N ratio (3.2) has the finest average austenite grain size (68 μm), followed by Steel 3 (78 μm) and

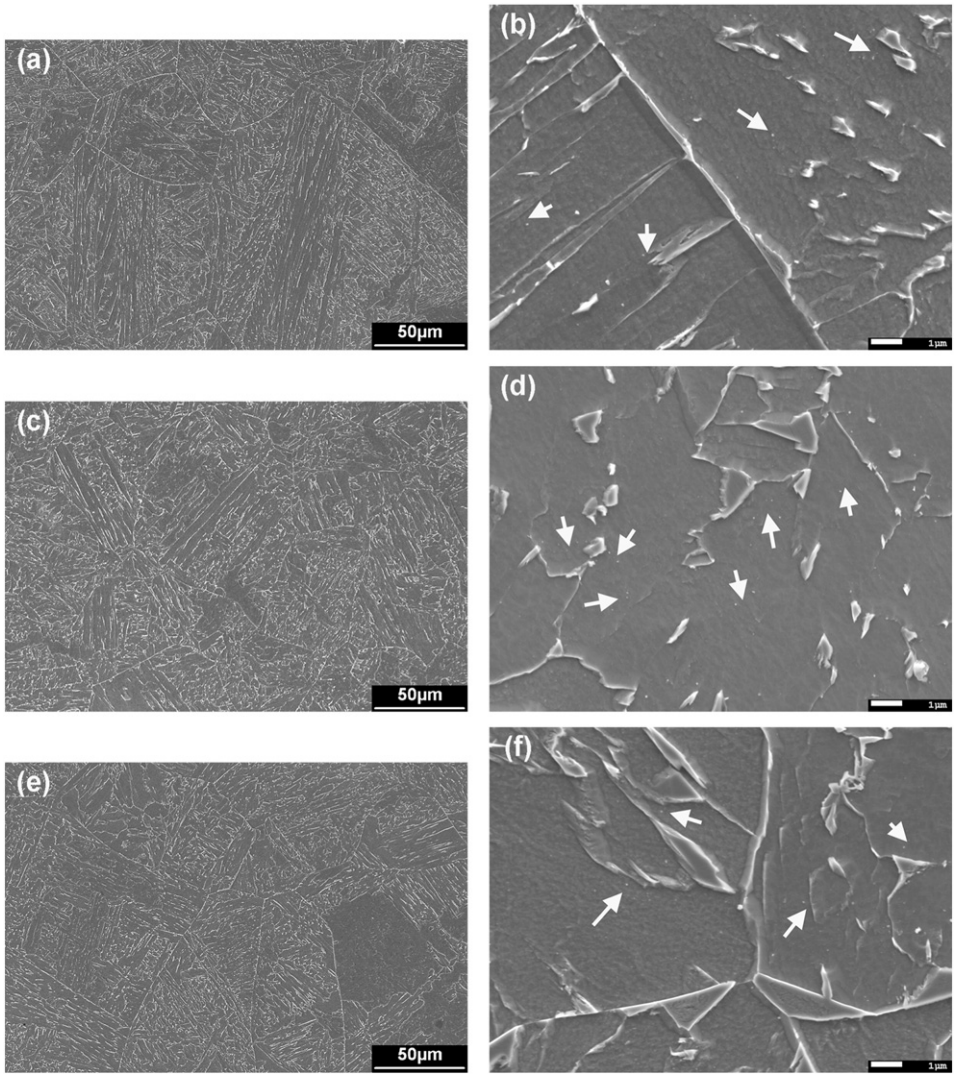

Fig. 3. Low magnification SEM micrographs (a, c & e) showing the microstructure and high magnification SEM micrographs (b, d & f) indicating the precipitates (as the arrows indicated) in simulated CGHAZ observed using field emission gun SEM for different Ti/N ratios (etched in 2% nital): (a)–(b) Ti/N = 1.9; (c)–(d) Ti/N = 3.2; (e)–(f) Ti/N = 4.9.

Table 2
Average austenite grain size and percentage of fine grains (<80 μm) in simulated CGHAZs of steels with different Ti/N ratios (the numbers in the brackets are standard deviations).

Steel no.	Ti/N ratio	Average grain size, μm	Percentage of fine grains (<80 μm)
1	1.9	84 (36)	51
2	3.2	68 (27)	71
3	4.9	78 (32)	59

Table 3
The average precipitates size and density of precipitates in simulated CGHAZs for steels with different Ti/N ratios (the numbers in the brackets are standard deviations).

Ti/N	Average precipitate size, nm	Density of precipitates, μm^{-2}
1.9	57 (20)	0.32
3.2	52 (24)	0.53
4.9	52 (24)	0.37

Steel 1 (84 μm). Moreover, Steel 2 had 71% of fine grains (i.e. finer than 80 μm), higher than the percentages of Steel 3 (59%) and Steel 1 (51%) respectively [25,26].

3.2. TEM study of precipitation

Plenty of bright field images were taken from a large area of the carbon replicas for the studied CGHAZ samples. The precipitate sizes were measured and calculated using image processing software. The size distribution of precipitates in each simulated CGHAZ was presented in Fig. 4. The TEM characterisation of CGHAZ carbon replicas revealed the presence of 20 to 160 nm-sized precipitates for all Ti/N ratios. As shown in Table 3, the average precipitate sizes of the three samples were at the same level (52–57 nm). It may be concluded that the variations in Ti/N ratio have no obvious impact on the precipitation behaviour in the CGHAZ. However, a close examination of the precipitate distribution suggested that the sample of Steel 2 with near-stoichiometric Ti/N ratio exhibited slightly higher percentage of fine precipitates (Fig. 4). Furthermore, the number density (numbers of precipitates per unit area) of the studied samples was calculated. As the precipitates are not uniformly distributed in the studied samples, five replicas were observed for each material to ensure that the density statistics was randomly from a large area. Hundreds of bright field images were randomly captured from many grids of the carbon replicas, irrespective of the number of precipitates in the image. Then added the numbers of precipitates counted from each image, divided by the sum of area all images covered, and the number density of precipitates was obtained for the comparison in this study. It is interesting to find that the number density of precipitates in the simulated CGHAZ of Steel 2 was significantly higher when compared to the others (Table 3).

As shown in Fig. 5, the TEM-EDS analysis of typical precipitates has shown that both the cuboidal and spheroidal particles contained Ti, Nb and V, but the EDS peaks of Ti were much higher than the peaks of Nb and V, indicating the precipitates observed were Ti-rich [26]. It should be noted that the peaks of Cu were from the Cu-grids that were used for supporting the carbon replicas. As shown in Fig. 6, some coarse precipitates larger than 200 nm were also occasionally observed [26]. This was due to the relatively low Ti and N contents in the steels studied, and thus significant TiN particle coarsening was not frequently observed in this study. The corresponding EDS analysis indicated that the coarse particles were Ti, Nb and V complex carbonitrides. Based on the observations and EDS analyses of all CGHAZ samples (not all presented here), the Ti/N ratio in the studied range does not evidently affect the morphology and chemical composition of particles in the simulated CGHAZ.

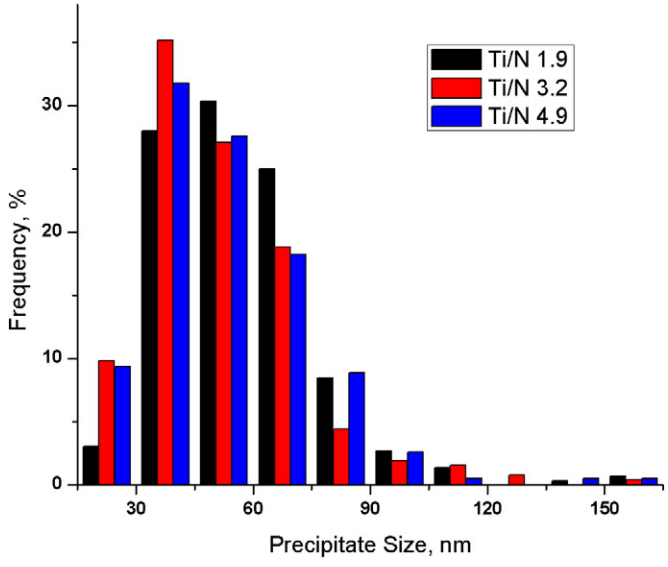

Fig. 4. The precipitate size distribution in simulated CGHAZs for various Ti/N ratios.

3.3. Mechanical properties

The Vickers hardness numbers, CVN impact energies and CTOD values of the simulated CGHAZ samples were summarised in Table 4. The hardness testing has shown no significant variation in the Vickers hardness (in a tight range of 211–214 HV_1) as a function of Ti/N ratio. The hardness values meet the requirements of line pipe specifications and far below the critical value (350 Vickers points) for the welding cold cracking [27]. The Charpy impact energy in the simulated CGHAZ of Steel 2 achieved the highest value (85 J) among the simulated CGHAZs of the studied steels. The relatively large standard deviation of the impact energy may be due to that the CVN testing temperature (−20 °C) was close to the ductile-brittle transition temperature (DBTT) of the studied materials. At the near-stoichiometric ratio, the simulated CGHAZ of Steel 2 exhibited the highest CTOD value (0.058 mm). Thus, the variation in the CTOD value tested at −20 °C for all the studied samples was similar to the trend of impact energy, which has been proven by numerous investigators [13,28–31], stating the positive correlation and transferability between CVN impact energy and CTOD value.

Fig. 7 shows the typical examples of SEM fractographs for fracture surfaces of the simulated CGHAZ after CVN testing. The evidence for cleavage fracture is clear for the simulated CGHAZ with different Ti/N ratios, which is indicated by the apparent river patterns with tearing ridges and flat facets observed in the central region of CVN fractured surfaces. The micrographs in Fig. 7a–c show relatively flat fracture surfaces, which is indicative of brittle fracture for different Ti/N ratios. The percentage of shear area was also evaluated for the fracture surfaces after CVN testing. As shown in the embedded macrographs in Fig. 7a–c, the percentage of shear area is estimated to be 30% (Steel 1), 40% (Steel 2) and 20% (Steel 3) respectively, which matches well with the values of CVN impact energy. Additionally, it is noted in the macrographs that the lateral deformation of different Ti/N ratios during the impact testing is slightly different. Sample of Steel 2 with Ti/N ratio of 3.2 exhibited the largest lateral deformation, followed by samples of Steel 1 and Steel 3. This is in accord with the CVN impact energy results that the highest average impact energy achieved in Steel 2 sample.

4. Discussion

According to the microstructural classification of Krauss et al. [32], in the studied samples the microstructural constituents inside the prior austenite grains were the major phase of bainitic ferrite and the minor secondary phase of M-A islands. Moreover, the transformation behaviour during the cooling process of HAZ thermo-mechanical simulation

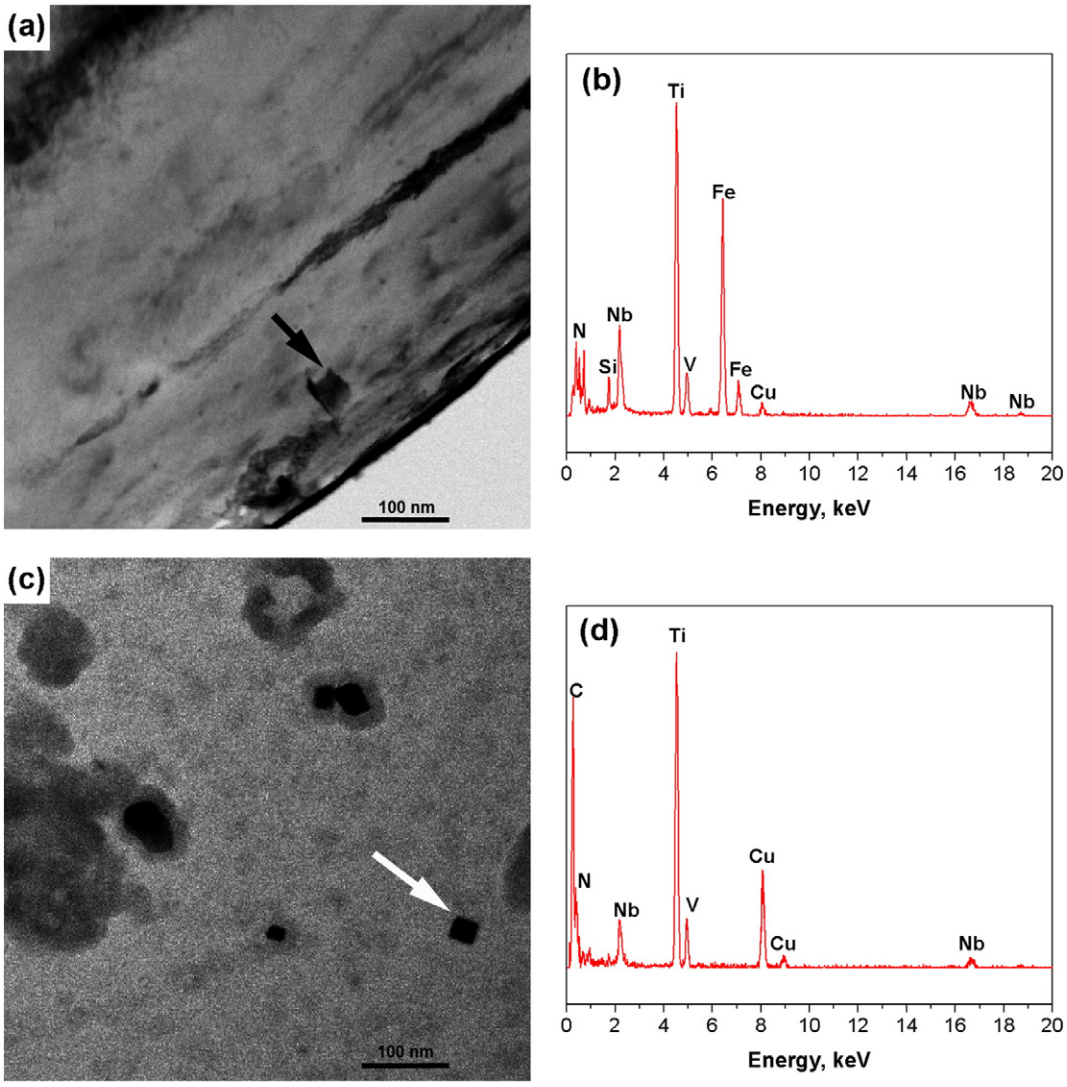

Fig. 5. Typical precipitates observed in the simulated CGHAZ and the corresponding EDS analyses (as the arrows in (a) and (c) indicated).

was estimated based on the chemical compositions and processing parameters. During cooling, bainitic ferrite was firstly formed as the dominant phase. The carbon diffused from the newly formed bainitic ferrite to the untransformed austenite and thus stabilised the austenite. With further cooling the austenite partially transformed into martensite, thus M-A islands formed (i.e. the mixture of martensite and retained austenite). Hence, this estimation was consistent with the microstructure of bainitic ferrite and M-A islands observed in the simulated CGHAZ (Fig. 3). Variations in Ti/N ratio therefore did not influence the type of microstructure constituents. This can be also supported from the hardness that is recognised to be a good indicator of microstructure. The hardness results revealed that the average hardness values of simulated CGHAZ with different Ti/N ratios were very similar and the corresponding standard deviations were small.

The presence of precipitates of microalloying elements can significantly influence the mechanical properties of line pipe steels, which is a function of the steel chemistry and processing parameters. In the current study, the steel samples were manufactured using the same processing parameters, which excluded the effect of processing. For the simulated CGHAZ, from the EDS analysis (Figs. 5 & 6), the majority of the precipitates were Ti-rich (Ti,Nb,V)(C,N) complex precipitates. This can be attributed to the relatively low free energy for TiN formation, high diffusion coefficient of Ti element in austenite, and thus high tendency to precipitate out compared to other microalloying elements such as Nb and V [33,34]. The microalloying elements such as Nb, Ti and V were almost uniformly distributed within the precipitates (Fig. 6). The average precipitate sizes in different Ti/N ratio samples were statistically calculated (Table 3) and levelled off at approximately 55 nm. One may claim that the Ti/N ratio exerted little effect on the precipitation behaviour in the studied steels. However, a close examination of the precipitate size distribution demonstrated that the sample of simulated CGHAZ with Ti/N ratio of 3.2 had slightly higher percentage of fine precipitates. Furthermore, at near-stoichiometric Ti/N ratio (3.2) the number density of precipitates in the simulated CGHAZ reached the maximum compared to the hypo- or hyper-stoichiometric ratios. It has been reported that for the initial composition, both its absolute value and its deviation from stoichiometric ratio of Ti and N are important in determining the amount of precipitation and the amount in solid solution [35]. For the studied samples, the Ti, N levels are controlled in a relatively tight range and other elements are constant, thus the influence of the initial chemical composition on precipitation among the three steels is marginal. Departure from the stoichiometry of Ti, N additions can alter the precipitation in quantity and hence affect properties [35]. Consequently, at near-stoichiometric Ti/N ratio more precipitates can pin the grain boundaries during the welding thermal cycle, leading to finer grain size and improved mechanical properties. This inference is well consistent with our previous study [25], which demonstrated that the sample of Steel 2 with Ti/N ratio of 3.2 (close to the stoichiometric

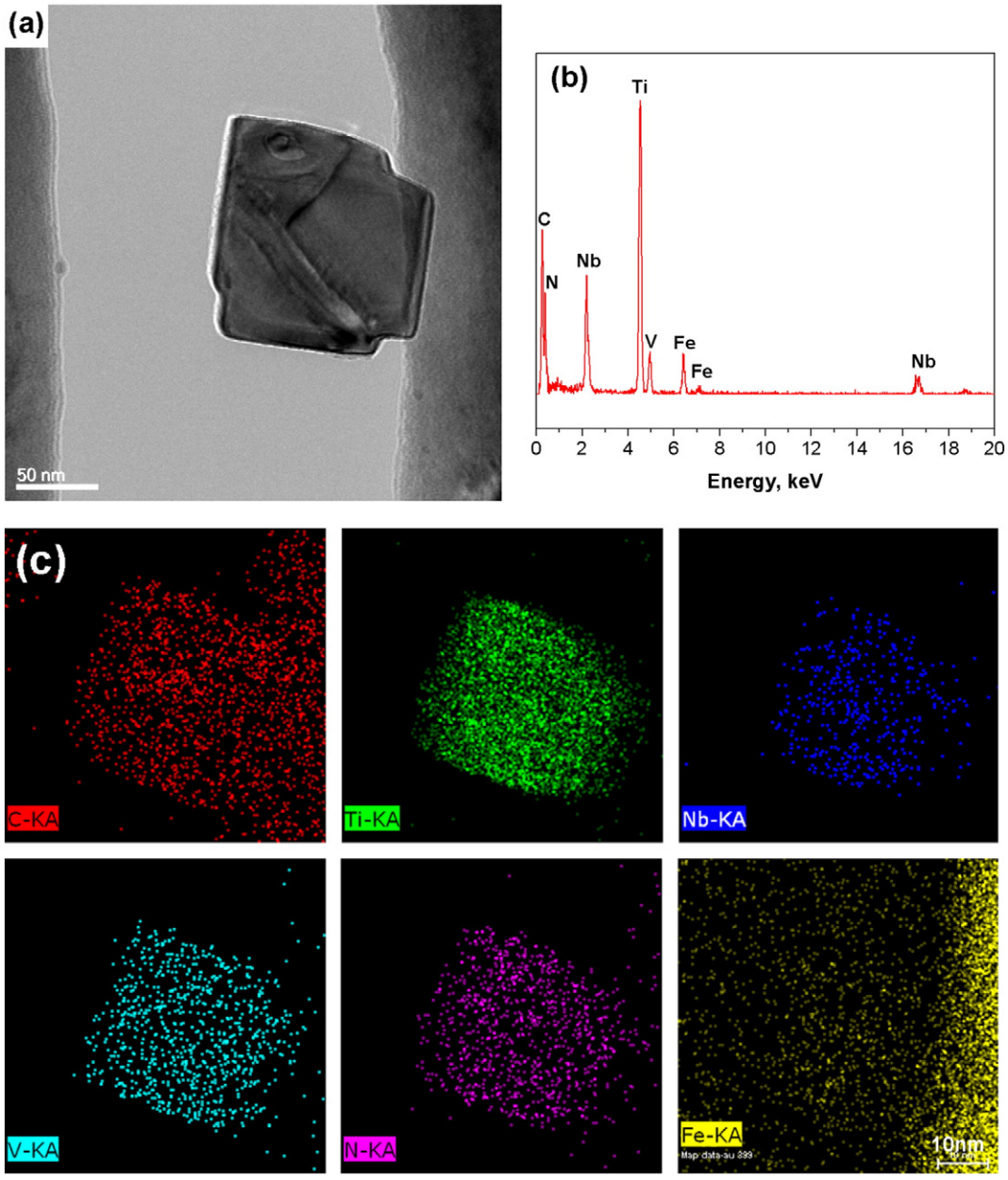

Fig. 6. TEM characterisation of typical coarse Ti–Nb–V complex precipitate in the simulated CGHAZ: (a) bright field image; (b) EDS spectrum; (c) EDS mapping analysis.

ratio) had slightly finer prior austenite grain size and higher fraction of fine austenite grains in the simulated CGHAZ. It is well known [36] that the relationship between TiN particles with the austenite grain size in microalloyed pipeline steels has been determined as:

$$R = k \cdot (r/f)$$

where R is the austenite grain size, k is the number factor depends on the particle type (for TiN precipitate, roughly 1.5), r is the size of particles and f is the volume fraction of particles. This suggests that for the effective control of grain size, the large volume fraction of small size particles is required. According to Pickering et al. [37], the grain coarsening temperature will be increased when there is a maximum volume fraction of pinning particles. The maximum grain coarsening temperature would occur at the stoichiometric Ti/N ratio where the temperature dependence on the solubility is greatest. In the present study, the sample of Steel 2 with near-stoichiometric Ti/N ratio is likely to achieve the lowest r/f value, which can bring about the high percentage of fine grains and improved mechanical properties.

Apart from the influence of Ti/N ratio, the amount of Ti precipitated is also essential for the properties of the studied steel samples. To further elucidate the mechanisms of alloy design of Ti and N, a thermodynamic equilibrium calculation was conducted based on the solubility product [38]. The equilibrium estimation of the amounts of Ti and N in solid solution and in precipitates at 1350 °C are summarised in Table 5. As expected and being consistent with above, the amount of Ti in precipitation for Steel 2 with near-stoichiometric Ti/N ratio is the highest among the studied steels, which suggests that larger amount of Ti-containing precipitates formed in Steel 2 and thus better

Table 4
The Vickers hardness numbers, CVN impact energies and CTOD values as a function of Ti/N ratio (the numbers in the brackets are standard deviations).

Ti/N	HV, load: 1 kg	CVN impact energy, J (tested at −20 °C)	CTOD value, mm
1.9	211 (6)	60 (39)	0.021 (0.003)
3.2	211 (2)	85 (40)	0.058 (0.017)
4.9	214 (6)	35 (14)	0.031 (0.002)

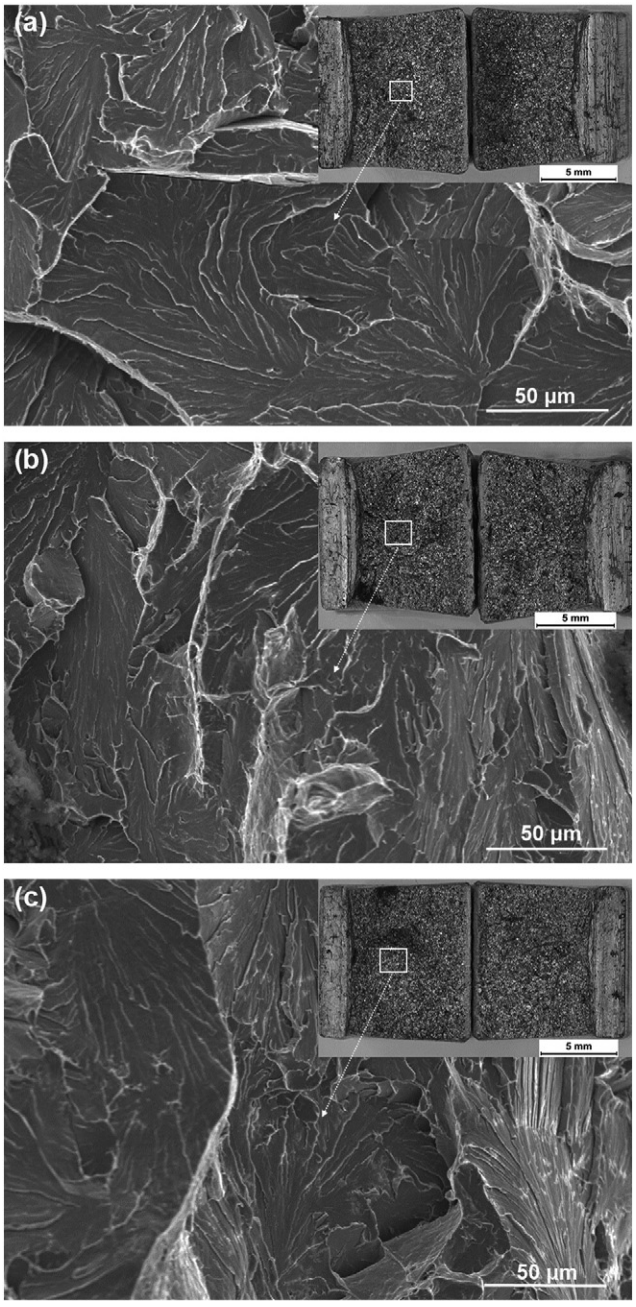

Fig. 7. The fracture surfaces after CVN testing observed using SEM: (a) Ti/N = 1.9; (b) Ti/N = 3.2; (c) Ti/N = 4.9.

toughness performance. By contrast, as shown in Table 5, the Ti in solution in Steel 3 with hyper-stoichiometric Ti/N ratio is the highest. This may increase the coarsening rate of Ti-rich particles, which can lower the efficiency of particle pinning effect and hence lead to grain growth in the HAZ [39]. However, the behaviour of precipitation coarsening was not observed in Steel 3, which presented almost similar precipitate size as Steel 1 and Steel 2, in spite of having a larger Ti/N ratio. From the equilibrium estimation in Table 5, the amount of Ti in precipitation for Steel 3 is the lowest. This is supported by the observation of the lower Ti-rich particle density in Steel 3, which was dominantly related to the lower N content. In term of hypo-stoichiometric Ti/N ratio in Steel 1, the amount of Ti in precipitation was obviously lower than Steel 2 having near-stoichiometric value. This is thought to be associated with the relatively lower Ti content, in spite of higher N concentration. Therefore, either high or low than the optimal Ti/N value can lead to slightly lower toughness due to reduced amount of Ti in precipitation at these Ti/N ratios.

Table 5
An equilibrium estimation of the amounts of Ti and N in solid solution ([Ti], [N]) and in precipitates (Ti_{ppt}, N_{ppt}) at 1350 °C, in wt.%.

Steel no.	Ti	N	Ti/N	[Ti]	[N]	Ti_{ppt}	N_{ppt}
1	0.0060	0.0032	1.9	0.0019	0.0020	0.0041	0.0012
2	0.0087	0.0027	3.2	0.0033	0.0011	0.0054	0.0016
3	0.0083	0.0017	4.9	0.0051	0.0008	0.0032	0.0009

The toughness of the simulated CGHAZ for the studied steels was evaluated using the CVN and CTOD testing. As shown in Fig. 8, the toughness results were correlated to the precipitation evolution and also the austenite grain size. Similar to the expectation based on the precipitation analysis and also the thermodynamic equilibrium estimation (Table 5), the results revealed that at near-stoichiometric ratio the maximum CVN impact energies and CTOD values were delivered in the samples of Steel 2. The observed higher number density of precipitates in the simulated CGHAZ of the steel with near-stoichiometric Ti/N ratio certainly contributed to the finer austenite grain size and hence improved CGHAZ toughness; whereas samples with both high and low Ti/N ratios exhibited reduced CGHAZ toughness due to insufficient amount of Ti precipitated. It is known that for microalloyed steels the Ti/N ratio plays a significant role in the HAZ toughness because of its influence on the austenite grain size [40]. In our study, high number density of precipitates achieved at the near-stoichiometric Ti/N ratio resulted in high percentage of fine austenite grains in the simulated CGHAZ [21]. The austenite grain boundaries are of significance in the cleavage fracture propagation [41]. For fine-grained steels, the increased number of grain boundaries can act to obstruct crack propagation and thus increase the energy required for fracture to propagate, thereby enhancing the toughness. This elucidated the better CGHAZ toughness performance of Steel 2 samples during the CVN and CTOD testing.

This work has demonstrated a marginal but important toughness increase in the CGHAZ achieved at Ti, N stoichiometry. Meanwhile, high number density of precipitates and then optimum control of austenite grain size in the weld HAZ were achieved when Ti/N ratio approached the stoichiometric ratio. This is very beneficial to the steelmaking and alloy design of line pipe steels. In terms of steel production, there should be a perceived benefit in seeking stoichiometry. It is apparent that the variable in steel production that is least controllable is the level of N. An appropriate specification should therefore aim at the lowest and

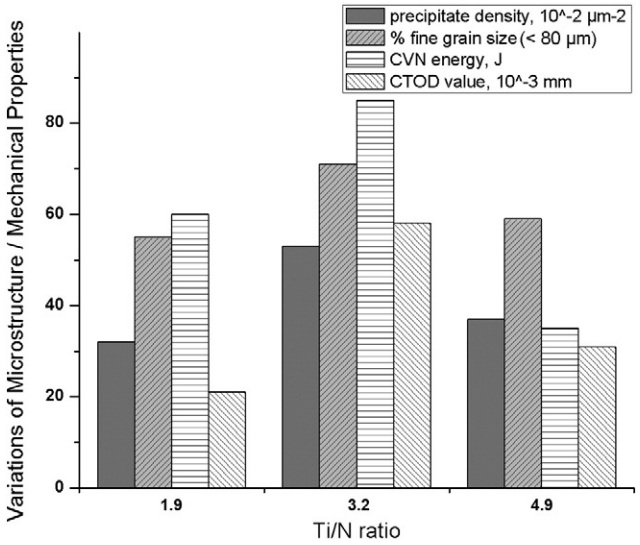

Fig. 8. Variations of CVN impact energy and CTOD value as a function of Ti/N ratio and correlation with the precipitation and austenite grains.

most consistent level of N. If it follows, then an appropriate Ti addition to achieve the needed stoichiometric ratio will be needed with respect to improved toughness performance.

5. Conclusions

In this present work, the variations in toughness of simulated CGHAZ as a function of Ti/N ratio were systematically explored through the CVN and CTOD testing and correlated to the precipitation evolution and austenite grain size. The microstructure of simulated CGHAZ for different Ti/N ratios consisted of bainitic ferrite and a small amount of M-A constituent within the prior austenite grains, irrespective of the Ti/N ratio. Nevertheless, samples of Steel 2 with near-stoichiometric ratio demonstrated the highest CVN impact energy and CTOD value among the studied range of Ti/N ratio, which is due to the increased number density of Ti–Nb–V precipitates in the CGHAZ and thus high percentage of fine austenite grains. The current work has identified a subtle difference in precipitation evolution and austenite grain coarsening in fundamentally identical steels with different Ti/N ratios. The implications of this work are significant in terms of optimal alloy design of steels for critical applications such as high-pressure pipelines.

Acknowledgements

Special thanks are extended to BaoSteel (China) for providing the materials to conduct this work. Thanks are due to Ewout Slachter for his contribution on the CTOD testing. The authors also acknowledge use of facilities within the UOW Electron Microscopy Centre, and appreciate the financial support from EPCRC for part of the work.

References

[1] X.W. Chen, G.Y. Qiao, X.L. Han, X. Wang, F.R. Xiao, B. Liao, Effects of Mo, Cr and Nb on microstructure and mechanical properties of heat affected zone for Nb-bearing X80 pipeline steels, Mater. Des. 53 (2014) 888–901.
[2] S. Liu, X. Li, H. Guo, C. Shang, R.D.K. Misra, Isolating contribution of individual phases during deformation of high strength–high toughness multi-phase pipeline steel, Mater. Sci. Eng. A 639 (2015) 131–135.
[3] B. Wang, C. Zhou, J.X. Zhu, X.Y. Tian, Study on continuous cooling transformation and strength-toughness of X70 pipeline steel with high deformability, Int J Microstructure Mater Properties 9 (2) (2014) 136–146.
[4] H. Xie, L.X. Du, J. Hu, R.D.K. Misra, Microstructure and mechanical properties of a novel 1000 MPa grade TMCP low carbon microalloyed steel with combination of high strength and excellent toughness, Mater. Sci. Eng. A 612 (2014) 123–130.
[5] R. Ghajar, G. Mirone, A. Keshavarz, Ductile failure of X100 pipeline steel — experiments and fractography, Mater. Des. 43 (2013) 513–525.
[6] E. Ei-Danaf, M. Baig, A. Almajid, W. Alshalfan, M. Al-Mojil, S. Al-Shahrani, Mechanical, microstructure and texture characterization of API X65 steel, Mater. Des. 47 (2013) 529–538.
[7] J.S. Lee, J.B. Ju, J.I. Jang, W.S. Kim, D. Kwon, Weld crack assessments in API X65 pipeline: failure assessment diagrams with variations in representative mechanical properties, Mater. Sci. Eng. A 373 (1–2) (2004) 122–130.
[8] J.I. Jang, Y. Choi, J.S. Lee, Y.H. Lee, D. Kwon, M. Gao, et al., Application of instrumented indentation technique for enhanced fitness-for-service assessment of pipeline crack, Int J Fracture 131 (2005) 15–34.
[9] H.K. Sung, S.Y. Shin, W. Cha, K. Oh, S. Lee, N.J. Kim, Effects of acicular ferrite on Charpy impact properties in heat affected zones of oxide-containing API X80 linepipe steels, Mater. Sci. Eng. A 528 (9) (2011) 3350–3357.
[10] S.H. Hashemi, Strength-hardness statistical correlation in API X65 steel, Mater. Sci. Eng. A 528 (3) (2011) 1648–1655.
[11] Y. Xu, K. Guan, Evaluation of fracture toughness by notched small punch tests with Weibull stress method, Mater. Des. 51 (2013) 605–611.
[12] J. Dziubiński, P. Adamiec, Correlations between Charpy V and crack tip opening displacement as well as drop weight teat test results, European Structural Integrity Society 30 (2002) 349–355.
[13] Y. Takashima, M. Ohata, F. Minami, Evaluation method for fracture mechanics-based material toughness from Charpy impact test, Mater. Sci. Forum 512 (2006) 61–66.
[14] J.H. Kim, S.W. Choi, D.H. Park, J.M. Lee, Charpy impact properties of stainless steel weldment in liquefied natural gas pipelines: effect of low temperatures, Mater. Des. 65 (2015) 914–922.
[15] C.L. Walters, A. Alvaro, J. Maljaars, The effect of low temperature on the fatigue crack growth of S460 structural steel, Int. J. Fatigue (2015) in press.
[16] J.B. Ju, W.S. Kim, J.I. Jang, Variations in DBTT and CTOD within weld heat-affected zone of API X65 pipeline steel, Mater. Sci. Eng. A 546 (2012) 258–262.
[17] A.A. Willoughby, Significance of pop-in fracture toughness testing, Int J Fracture 30 (1) (1986) R3–R6.
[18] M. Koçak, L. Chen, G. Terlinde, G. Gnirss, K.H. Schwalbe, CTOD testing of HAZ and analysis of pop-in behavior, J Offshore Mech Arctic Eng 112 (3) (1990) 214–222.
[19] Z. Zhu, L. Kuzmikova, H.J. Li, F. Barbaro, Effect of inter-critically rehearing temperature on microstructure and properties of simulated inter-critically reheated coarse grained heat affected zone in X70 steel, Mater. Sci. Eng. A 605 (2014) 8–13.
[20] S.F. Medina, M. Chapa, P. Valles, A. Quispe, M.I. Vega, Influence of Ti and N contents on austenite grain control and precipitate size in structural steels, ISIJ Int. 39 (9) (1999) 930–936.
[21] I. Rak, V. Gliha, V. Koçak, Weldability and toughness assessment of Ti-microalloyed offshore steel, Metall Mater Trans A 28 (1) (1997) 199–206.
[22] S.C. Wang, The effect of titanium and nitrogen contents on the microstructure and mechanical properties of plain carbon steels, Mater. Sci. Eng. A 145 (1) (1991) 87–94.
[23] M. Okatsu, K. Oi, K. Ihara, T. Hoshino, High strength linepipe with excellent HAZ toughness, Proceedings of ASME 2004 23rd International Conference on Offshore Mechanics and Arctic Engineering, Vancouver, Canada; June 20–25, 2004.
[24] Zhu Z, Kuzmikova L, Marimuthu M, Li HJ, Barbaro F. Role of Ti and N in line pipe steel welds. Sci. Technol. Weld. Join. 2013; 18(1): 1–10.
[25] Z. Zhu, M. Marimuthu, L. Kuzmikova, H.J. Li, F. Barbaro, L. Zheng, et al., Influence of Ti/N ratio on simulated CGHAZ microstructure and toughness in X70 steels, Sci. Technol. Weld. Join. 18 (1) (2013) 45–51.
[26] Z.X. Zhu, Structure Property Correlation in the Weld HAZ of High Strength Line Pipe Steels. Doctor of Philosophy Thesis, University of Wollongong, Wollongong, 2013.
[27] W.A. Bruce, M.A. Boring, Comparison of methods for predicting safe parameters for welding onto in-service pipelines, 2006 International Pipeline Conference, Calgary, Canada; September 25–29, 2006.
[28] W. Tyson, S. Xu, R. Bouchard, Correlation between J and CVN in upper shelf, European Structural Integrity Society 30 (2002) 325–332.
[29] J. Dziubiński, P. Adamiec, Correlations between Charpy V and crack tip opening displacement as well as drop weight tear results, European Structural Integrity Society 30 (2002) 349–355.
[30] G. Puppala, A. Moitra, S. Sathyanarayanan, R. Kaul, G. Sasikala, R.C. Prasad, et al., Evaluation of fracture toughness and impact toughness of laser rapid manufactured Inconel-625 structures and their co-relation, Mater. Des. 59 (2014) 509–515.
[31] Minami F. Transferability of Charpy absorbed energy to fracture toughness based on Weibull Stress Criterion. J. Mater. Sci. Technol. 2005; 1: 1–4.
[32] G. Krauss, S.W. Thompson, Ferritic microstructures in continuously cooled low- and ultralow-carbon steels, ISIJ Int. 35 (8) (1995) 937–945.
[33] H. Zou, J. Kirkaldy, Carbonitride precipitate growth in titanium/niobium microalloyed steels, Metall Trans A 22 (7) (1991) 1511–1524.
[34] A. Craven, K. He, L. Garvie, T. Baker, Complex heterogeneous precipitation in titanium-niobium microalloyed Al-killed HSLA steels-I(Ti, Nb)(C, N) particles, Acta Mater. 48 (15) (2000) 3857–3868.
[35] Wadsworth J, Woodhead J, Keown S. The influence of stoichiometry upon carbide precipitation. Metal Sci 1976; 10(10): 342–8.
[36] S. Matsuda, N. Okumura, Effect of distribution of Ti nitride precipitate particles on the austenite grain size of low carbon and low alloy steels, Trans Iron Steel Inst Jpn 18 (4) (1978) 198–205.
[37] F. Pickering, Titanium nitride technology, Proceedings of the 35th Mechanical Working and Steel Processing Conference, Pittsburgh, USA, 1993.
[38] J. Strid, K.E. Easterling, On the chemistry and stability of complex carbides and nitrides in microalloyed steels, Acta Metall. 33 (11) (1985) 2057–2074.
[39] W. Yan, Y.Y. Shan, K. Yang, Effect of TiN inclusions on the impact toughness of low-carbon microalloyed steels, Metall Mater Trans A 37 (7) (2006) 2147–2158.
[40] T. McGurk, J. Speer, D. Matlock, Effect of alloy modifications on HAZ microstructure and properties of HSLA X80 pipeline steel, Mater. Sci. Technol. 6 (2006) 347.
[41] S. Kim, S. Lee, B.S. Lee, Effect of grain size on fracture toughness in transition temperature region of Mn-Mo-Ni low-alloy steels, Mater. Sci. Eng. A 359 (1) (2003) 198–209.